

Potential impact of climate change on intensity duration frequency curves of central Alberta

Chun-Chao Kuo · Thian Yew Gan · Mesgana Gizaw

Received: 25 February 2014 / Accepted: 30 January 2015 / Published online: 18 February 2015
© Springer Science+Business Media Dordrecht 2015

Abstract Under the effect of climate change, warming likely means that there will be more water vapour in the atmosphere and extreme storms are expected to occur more frequently and with greater severity, resulting in municipal Intensity-Duration-Frequency (IDF) curves with higher intensities and shorter return periods. A regional climate model, MM5 (the Pennsylvania State University / National Center for Atmospheric Research numerical model), was set up in a one-way, three-domain nested framework to simulate future summer (May to August) precipitation of central Alberta. MM5 is forced with climate data of four Global Climate Models, CGCM3, ECHAM5, CCSM3, and MIROC3.2, for the baseline 1971–2000 and 2011–2100 based on the Special Report on Emissions Scenarios A2, A1B, and B1 of Intergovernmental Panel on Climate Change. Due to the bias of MM5's simulations, a quantile-quantile bias correction method and a regional frequency analysis is applied to derive projected grid-based IDF curves for central Alberta. In addition, future trends of air temperature and precipitable water, which affect storm pattern and intensity, are investigated. Future IDF curves show a wide range of increased intensities especially for storms of short durations (≤ 1 -h). Conversely, future IDF curves are expected to shift upward because of increased air temperature and precipitable water which are projected to be about 2.9 °C and 29 % in average by 2071–2100, respectively. Our results imply that the impact of climate change could increase the future risk of flooding in central Alberta.

1 Introduction

Central Alberta experienced numerous severe storms in 2004, 2009, and 2012, which resulted in considerable damages such as flooded basements, sewage backups, overflows in wastewater treatment plants, damaged roadways, and sewage discharge into waterways according to the Canadian Disaster Database (<http://www.publicsafety.gc.ca/cnt/rsrscs/cndn-dsstr-dtbs/index-eng.aspx>). The damage due to storm events of 2004 and 2012 for the city of Edmonton resulted in about 160 million CAD (Environment Canada 2014) and 106 million CAD

Electronic supplementary material The online version of this article (doi:10.1007/s10584-015-1347-9) contains supplementary material, which is available to authorized users.

C.-C. Kuo (✉) · T. Y. Gan · M. Gizaw
Department of Civil & Environmental Engineering, University of Alberta, Edmonton, AB T6G 2W2,
Canada
e-mail: chunchao@ualberta.ca

(Insurance Bureau of Canada 2012) insurance claims, respectively. In addition, about thirty thousand residents of Edmonton were evacuated because of the 2004 storm event. Based on the past IDF curves (1914–1995), the maximum observed 1-hour rainfall (48.9 mm) of the 2012 event is estimated to have a return period of over 200-year. The 4-h and 24-h storm intensities are estimated to have return periods of 10-year and 2-year, respectively. The return periods of them are smaller than that of 1-h storm intensity because this storm event is only 1 h. Given that municipal drainage pipes are designed against storms of 5-year return period and 4-h duration, while retention ponds are designed against storms of 100-year return period and 24-h duration, it seems that recent extreme storms are capable of overwhelming existing municipal structures of central Alberta. The potential evolution of local climatic regimes must therefore be taken into consideration when designing new municipal structures and developing future flood contingency plans for central Alberta.

A growing number of studies show that precipitation variability is increasing globally as our planet warms (e.g., Dore 2005; IPCC 2007 and 2013). In other words, global warming can potentially cause future extreme storm events to occur more frequently and in greater severity. Indeed, warmer temperatures have been linked to increasing rainfall intensities in many parts of the world (Hamlet and Lettenmaier 2007; Allan and Soden 2008; Lenderink and Meijgaard 2008; Wang et al. 2008). Many studies (e.g., Mekis and Hogg 1999; Zhang et al. 2000; Groisman and Rankova 2001; Alexander et al. 2006; Subash et al. 2011; Wang et al. 2013) showed that increasing precipitation had been observed in the Northern Hemisphere in mid- and high-latitudes over past several decades. Shi and Xu (2008) found that about 54.3 % of global terrestrial areas experienced increasing annual precipitation between 1951 and 2002.

From examining precipitation simulated under various IPCC (Intergovernmental Panel on Climate Change) emissions scenarios of the Fourth Assessment Report (AR4), Sun et al. (2007) concluded that all projections suggested more extreme precipitation behavior globally, where wet regions might be getting wetter while arid regions may be getting drier. The Fifth Assessment Report (AR5) of IPCC (2013) also concluded that more regions experienced increased heavy precipitation (above the 95th percentile) events at daily and sub-daily scales since 1951. Precipitation patterns are likely changing, but due to intrinsically high spatial and temporal variabilities of precipitation, many details pertaining to these changes remain uncertain. For example, extreme storm intensities are projected to increase in some areas even though seasonal summer precipitation is generally projected to decrease, as what had been observed in the summer season of Europe for the last several decades (Christensen and Christensen 2003; Khon et al. 2007; Kysely et al. 2012). In other words, global warming could potentially change existing Intensity-Duration-Frequency (IDF) curves, which have been extensively used in Canadian cities to estimate intensities of storms with specified return periods (frequency) and durations. Such potential changes could have significant implications to the safety standard of existing municipal infrastructure developed on the basis of existing IDF curves.

Traditionally, IDF curves developed out of historic precipitation data are assumed to be stationary, which means that future climate is assumed to remain unchanged. Realistically, existing IDF curves of Canadian cities derived from historical data are likely obsolete or not representative of future precipitation regimes because under the impact of climate change, extreme storms are mainly expected to occur more frequently and in greater intensity. By developing IDF curves that incorporate possible changes to climatic regimes because of warming, we will be better prepared to adapt to the potential impact of climate change.

Global Climate Models (GCMs) are designed to simulate global scale climate processes but at resolutions (from $1.1^\circ \times 1.1^\circ$ to $2.8^\circ \times 2.8^\circ$ for the four GCMs used in this study) not sufficient to account for details of local scale precipitation-producing weather systems. By

applying a regional climate model (RCM) driven with boundary conditions simulated by GCMs, we could simulate the behavior of local climate systems subjected to global scale climate processes simulated by GCMs forced with anthropogenic greenhouse gases. In other words, we could take advantages of both RCMs and GCMs to sort out the detailed behavior of local scale precipitation-producing weather systems of smaller areas under the impact of climate change in a global domain. Conversely, based on the simulations of RCMs, corrected due to bias and differences of spatial scale, we could project possible changes to precipitation at high temporal and spatial resolutions. With precipitation outputs of MM5 at 15-minute time steps, we can estimate intensities of short duration storms in the IDF curves, up to 15-minute durations. Further, setting up Domain 3 at 3 km resolution can adequately account for the spatial variability of rainfall of central Alberta at local scales.

The precipitation over Canada under the potential impact of global warming has been assessed using both GCMs and RCMs (Laprise et al. 2003; Mladjic et al. 2011; Mailhot et al. 2012; Sillmann et al. 2013). Shepherd and McGinn (2003) found that annual precipitation of Alberta will significantly increase with the largest increase in central Alberta, while for the future trend of annual maximum precipitation in storms of 6-h, 12-h, 24-h, 72-h, and 120-h durations, Mailhot et al. (2012) also found that they will increase in Canadian Prairies. However, existing studies on the intensity of future extreme storms and IDF curves in Alberta needed for engineering planning and design are limited at daily and multi-day time scales (e.g., Mailhot et al. 2010; Sillmann et al. 2013).

According to results of CMIP5 (Coupled Model Intercomparison Project Phase 5), with respect to 1981–2000 as the reference period, the climate of central Alberta is projected to become more extreme in 2081–2100 (Sillmann et al. 2013). The precipitation indices R95p (annual total precipitation when daily precipitation is greater than the 95th percentile of precipitation on wet days) and R10mm (number of days where the daily precipitation is greater than 10 mm) are projected to increase by about 10–70 % and 0.5–4 days in 2081–2100, respectively. By statistically downscaling the climate projections of CGCM3 using a quantile-based approach for the city of Saskatoon, Hassanzadeh et al. (2014) also found that climate change is projected to result in higher intensities of storms of short durations (1-h and 6-h) and small return periods (≤ 10 -year). Similarly, using climate projections of CGCM3, Mailhot et al. (2010) did not detect much change to intensities of annual maximum storms of long durations (e.g., 24-h) in the Canadian Prairies by 2081–2100.

2 Research objectives

In view of the potential impact of climate change on precipitation regimes and the need to update IDF curves of central Alberta, this study has two objectives:

- (1) Using a RCM, MM5 (the Pennsylvania State University / National Center for Atmospheric Research numerical model), dynamically downscale climate data of four GCMs (CGCM3, ECHAM5, CCSM3 and MIROC3.2) for the baseline 1971–2000, and the SRES (Special Report on Emissions Scenarios) A2, A1B, and B1 scenarios of three future periods, 2011–2040 (2020s), 2041–2070 (2050s), and 2071–2100 (2080s), to project future sub-daily precipitation of central Alberta at high spatial resolutions. Each SRES scenario represents different projected rate of population and economic growth, technology development, level of environment protection, etc., in the future.

- (2) On the basis of MM5's simulations, estimate future trend slopes of air temperature and precipitable water using the Theil-Sen Estimator (Theil 1950; Sen 1968), and investigate potential changes of future IDF curves of Edmonton are for 2011–2100.

A flowchart of this study is shown in Fig. S1. MM5 was driven with initial and lateral boundary conditions taken from four GCMs to simulate local scale climate processes of central Alberta for the baseline (1971–2000) and projected periods (2011–2100). Next, future changes of 2-m air temperature and precipitable water were estimated using the Delta change method while future IDF curves were estimated after a Quantile-Quantile bias correction was applied to MM5's simulations.

3 Data

3.1 Rain gauge data

The study site, city of Edmonton in central Alberta, has a land area of about 701 km². Edmonton, with a fairly dense rain gauge network spreading across the city, has 13 rain gauges with high-quality records from May to August (MJJA) available for analysis between 1984 and 2010 (Fig. 1). Only the MJJA data were checked for quality control but not records outside of these 4 months so they were not included in this study. The rain gauge data (RG) of Edmonton are recorded at 5-min intervals. Because MJJA is the major raining season of central Alberta, with a seasonal average of 219.5 mm, rainfall records from MJJA dominated by short duration storms have been mostly used to design the infrastructure of Edmonton. Figure S2 shows the probability distribution of storm durations for MJJA (May to August) between 1984 and 2010. A storm event is defined on the basis of hourly time scale, which means that two set of rainfall records are divided and defined as two separated storm events if there is at least 1 h of non-rainfall period between them. Figure S2 shows that about 93 % of storm durations of MJJA between 1984 and 2010 occurred within 4 h.

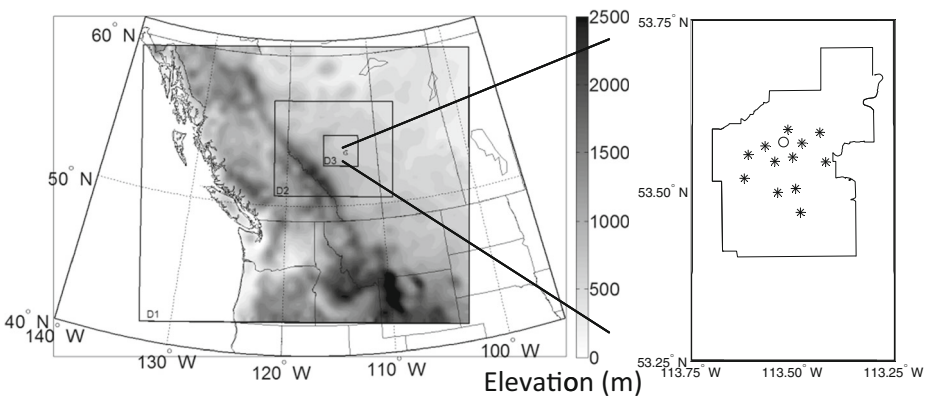


Fig. 1 MM5 domain outlines (encompassed by the *thin black lines*) and Edmonton area with its 13 rain gauges (*circle*: Municipal Airport rain gauge; *star*: new rain gauges) locations

3.2 Data from global climate model

6-hourly climate data of four GCMs, CGCM3 (3rd generation Canadian GCM), ECHAM5 (5th generation, German GCM), CCSM3 (Version 3 of the Community Climate Systems Model of USA), and MIROC3.2 (Version 3.2 of the Japanese GCM, Model for Interdisciplinary Research on Climate), were dynamically downscaled by MM5. The climate data required include geopotential height, specific humidity, air temperature, wind fields, surface pressure, mean sea level pressure, and sea surface temperature. All selected GCMs include climate data of the IPCC 20th Century experiment (20c3m) of 1850–2000, and the three 2001–2100, SRES climate projections, A1B, A2, and B1. The SRES A2 scenario projects the highest increase in air temperature while the SRES B1 scenario projects the most modest increase (IPCC 2007). The increase of mean air temperature under the SRES A1B scenario is in between that of SRES A2 and B1 scenarios.

The CGCM3 of the T47 version, with a resolution of about 3.75 degrees in both latitude and longitude directions, only has climate data for SRES A2 and A1B scenarios, MIROC3.2 of higher resolution version (hires), with roughly 1.1 degrees in latitude and longitude directions, only has climate data for SRES A1B and B1 scenarios, but ECHAM5 and CCSM3 have climate data for all three SRES scenarios. Therefore, in this study 10 sets of SRES scenario data were downscaled using MM5 for central Alberta.

4 Methodology

4.1 RCM configurations and post-processing

MM5 was first run for 30 May–August periods (4-month) between 1971 and 2000 using a one-way nesting with a 3-domain configuration, and four GCM outputs (see Section 3.2) were used as initial and lateral boundary conditions for the outermost domain (D1) at 27-km resolution. The D1 output was used to run the second domain (D2) of 9-km resolution, and D2 output was used to run the 3-km resolution, innermost domain (D3). The locations of the three domains with terrain elevation inside D1 and D2 are shown in Fig. 1. All these three domains were run with 23 vertical levels.

Erfani et al. (2003), who used the Global Environmental Multiscale (GEM) model of Environment Canada to examine features of a summertime supercell storm in central Alberta, found that a 4-km resolution model domain was sufficient to credibly simulate the climate system initiated along the Rocky Mountain foothills. Thus, our spatial resolutions should be sufficient to resolve the small-scale convective precipitation events that are common in Alberta during summers, and so no cumulus parameterization was used in D2 and D3. The high-resolution, Blackadar planetary boundary layer (PBL) scheme, the mixed-phase (Reisner 1; Reisner et al. 1998) explicit moisture scheme, and the rapid and accurate radiative transfer model longwave radiation scheme (RRTM; Mlawer et al. 1997) were used in this study. Because the 27-km spatial resolution of D1 was not sufficient to resolve the small-scale convective precipitation events, the Kain-Fritsch 2 (Kain 2004) cumulus parameterization was applied in this outermost domain. Given that developing IDF curves require sub-hourly precipitation data, output of MM5 at 15-minute time intervals for the innermost domain (D3) was used to estimate the grid-based IDF curves. These settings were used for simulating both the climate baseline period 1971–2000 and for the future period 2011–2100 using GCM outputs.

The area where future projections of air temperature and precipitable water were analyzed was located in the Domain 3 (D3), but the data within about 30 km length to the boundary of D3 were discarded to avoid the influence of boundary effects to climate variables. The simulated 2-m air temperatures in D3 were spatially and temporally averaged for the MJJA season. Next, the MJJA air temperature anomaly time series for 2011–2100 were estimated from subtracting MM5's simulation with the simulated average MJJA air temperature of 1971–2000. The time series representing the change of precipitable water (ratio) over 2011–2100 was estimated by dividing precipitable water simulated by MM5 for 2011–2100 by the average value of 1971–2000. All the trend analyses were tested using the Mann-Kendall trend test (Mann 1945; Kendall 1975) with a 0.05 significance level. The slope of trends was calculated using the Theil-Sen Estimator (Theil 1950; Sen 1968).

4.2 Intensity-duration-frequency curves and the bias correction

The IDF curves for the base period (1984–2010) was estimated from the annual maximum observed precipitation of various storm durations derived from the raw 5-minute precipitation data of the City of Edmonton. Out of a total of 13 gauges, nine rain gauges were in operation for 1984–2010, two rain gauges operated for 26 years, and two other rain gauges operated for 21 and 22 years, respectively. Based on results obtained from the heterogeneity measure of Hosking and Wallis (1997) applied to these 13 rain gauge data, this region is identified as homogeneous. Further, on the basis of results obtained from the Mann-Kendall test applied at a 0.05 significance level, more than 98 % of the 1984–2010 time series can be considered as stationary.

We developed IDF curves from precipitation data simulated by MM5 for storm durations ranging from 15 to 30-min, 1-h, 2-h, 4-h, 6-h, 12-h and 24-h, and for return periods of 2, 5, 10, 25, 50, and 100-year. Annual maximum rainfall intensity was obtained by the moving window method for the MJJA season only, which we refer to as AMI-MJJA. The AMI-MJJA for storm durations other than 15-min was obtained by the moving window method applied to the AMI-MJJA data at 15-min intervals. The AMIs-MJJA of each storm durations were fitted using a GEV (Generalized Extreme Value) probability distribution function with parameters estimated using the PWM (Probability Weighted Moment) method (Kuo et al. 2013 and 2014). Based on the probability distribution functions computed for the aforementioned storm durations, single-site and multi-site IDF curves were estimated. The results are presented in terms the upper (maximum) bound of IDF curves computed from rain gauges (within the right plane of the Fig. 1) and from the simulations of MM5. By showing the upper and lower bounds of IDF curves, the uncertainty associated with the projection of future IDF curves based on 10 sets of climate data of four GCMs and three SRES scenarios dynamically downscaled by MM5 were estimated.

Because storms simulated by MM5 tended to suffer from over-simulation (positive bias), a quantile-quantile bias correction (Boé et al. 2007; Sun et al. 2011; Johnson and Sharma 2011; Xu and Yang 2012) approach was applied to MM5's simulations before the data can be used to estimate IDF curves. In this method, a “quantile map” for both the simulated and observed precipitation data of the same period were created by applying an unbiased quantile estimator (Lafon et al. 2013) to ranked data, i.e., a X value simulated by MM5 was associated with a cumulative probability, p , of the Cumulative Distribution Function (CDF) of MM5's simulated rainfall intensity (Fig. S3). Next, from the CDF of observed precipitation, the quantile value, X' , with the same p was the bias corrected value. By applying this bias correction approach, bias corrected precipitation simulated by all 194 grids defined by MM5 within Edmonton area in D3 were derived which were used to develop the grid-based IDF curves of Edmonton using

the regional frequency analysis (RFA) framework of Hosking and Wallis (1997). Before the bias correction, there were obvious discrepancies between regional IDF curves estimated from the RFA of Hosking and Wallis (1997) using simulations of MM5 driven with climate data of four GCMs and the regional IDF curves derived from rain gauge precipitation data collected in 1984–2000 (see Tables S1–S2). With respect to regional IDF curves derived from rain gauge precipitation, the regional IDF curves derived from MM5's simulations forced by outputs of CGCM3 (Canada) and CCSM3 (USA) have lower levels of discrepancy than those derived by MM5 forced by outputs of two other GCMs, ECHAM5 (Germany) and MIROC3.2 (Japan).

5 Discussion of results

5.1 Future projections of 2-m air temperature and precipitable water

The increase of greenhouse gases leads to increased air temperature (IPCC 2007), which increases the atmosphere's capacity to accommodate more precipitable water, thus providing an environment suitable for the development of more extreme storms. Therefore, we discuss the change of air temperature and precipitable water in this section.

The spatially averaged, 2-m annual air temperature anomaly time series at D3 for MJJA simulated by MM5 are shown in Fig. 2a. Shaded red, blue, and green plots represent the range of temperature projected by MM5 driven by 4 GCMs under SRES scenarios of A2, A1B, and B1 in 2011–2100, respectively. The temperature anomaly time series simulated for 2011–2100 shows consistent increasing (positive) trends which imply that central Alberta is projected to become increasingly warmer over the 21st Century. The projected rates of increase that range between 0.011 and 0.052 °C/year in 2011–2100 are based on all the rates estimated from SRES scenarios of 4 GCMs using the Theil-Sen estimator (see Fig. S4). By 2020s, the projected increase in air temperature ranges from –0.1 to 2.3 °C with an average increase of

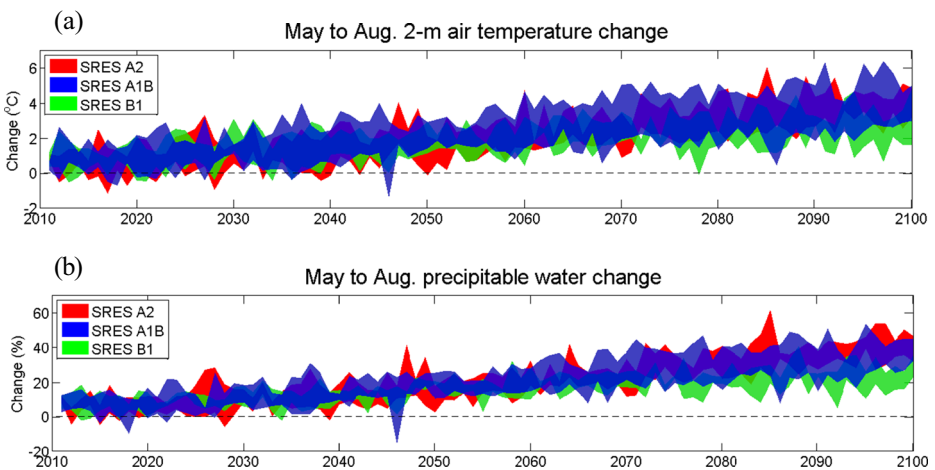


Fig. 2 **a** The annual anomaly time series of simulated D3's (Domain 3) May to Aug. 2-m temperature (temperature in the future – temperature in baseline period) (°C) projected by MM5 driven by 4 GCMs under SRES A2, A1B, and B1 scenarios. **b** The annual anomaly time series of simulated D3's (Domain 3) May to Aug. precipitable water (pwt) (%) ((pwt in the future – pwt in basis period) / (pwt in basis period) × 100 %) projected by MM5 driven by 4 GCMs under SRES A2, A1B, and B1 scenarios

about 1.0 °C. By 2080s, air temperature is projected to increase between 1.4 and 4.9 °C, with an average projected increase of about 2.9 °C. All three SRES scenarios, A2, A1B and B1 project similar range of temperature increase in central Alberta in the 2020s and the 2050s. However, for the 2080s, A2 and A1B scenarios projected a higher increase in air temperature, but B1 scenario only projects a modest increase. Overall, these 10 anomaly time series of 2-m air temperature exhibit increasing trends in 2011–2100 that, based on the Mann-Kendall trend test, are statistically significant at a 0.05 significance level.

The spatially averaged, precipitable water annual anomaly time series at D3 for the MJJA season simulated by MM5 for SRES A2, A1B, and B1 scenarios also consistently show increasing trends similar to the projected 2-m air temperature. In Fig. 2b, the shaded colors represent the range of projected precipitable water change expressed in percentage for all three dynamically downscaled SRES scenarios using simulations of four GCMs as initial and boundary conditions. The projected rates of increase in precipitable water range from 0.125 to 0.485 %/year in 2011–2100. The simulated time series of 2-m air temperature change and trends are shown in Fig. S5. The projected increase in precipitable water ranges from about 0.5 to 18.6 % with an average of 9.4 % in the 2020s, and about 14.9 to 43.8 % with an average of 28.9 % in the 2080s.

All three SRES scenarios, A2, A1B and B1 project similar range of precipitable water increase in central Alberta in the 2020s and the 2050s. However, in the last decade of the 21st century, A2 and A1B scenarios project higher increase in precipitable water, with an average of about 34.8 %, while the B1 scenario projects an average increase of about 28.1 %. Overall, based on the Mann-Kendall's test at a 0.05 significance level, the increasing trends of precipitable water over 2011–2100 are statistically significant.

5.2 Comparisons between the past (1914–1995), present (1984–2010) and future (2011–2100) IDF curves

First, we examined differences between the past (1914–1995) and the present (1984–2010) IDF curves of Edmonton. Gauge rainfall data at the Edmonton Municipal Airport were used to estimate the past IDF curves. The rainfall records at this rain gauge and other twelve rain gauges were used to estimate the present IDF curves as shown in Fig. 1. The former IDF curves developed by the city of Edmonton were based on the EVI-MOM method (quantiles were derived from the Extreme Value Type I probability distribution with parameters derived using the method of moment), and single-site observations collected at the municipal airport (shown as blue dash lines in Fig. 3). The latter IDF curves were estimated from 13 stations of rainfall data collected within the city of Edmonton using the GEV-PWM method. The upper bound of the 13 sets of IDF curves were chosen as the IDF curves representing the annual maximum rainfall (solid black curves in Fig. 3). For return periods less than 10-year, intensities of storms of short durations (≤ 1 -h) based on the past and the present IDF curves of Edmonton are similar to each other. However, intensities of long duration storms (> 1 -h) based on the present IDF curves are marginally smaller than those based on the past IDF curves. For return periods larger than 10-year, intensities of storms of all durations based on the present IDF curves are consistently higher than those based on the past IDF curves.

The present IDF curves developed out of the 1984–2010 rain gauge data of Edmonton seem to be consistent with several extreme storms that lead to flooding in Edmonton in July 2004, 2009 and 2012, respectively. Furthermore, in recent years, many extreme storm events occurred in Canada, such as the June, 2013 flood of Calgary (Southern Alberta) and the July, 2013 flood of Toronto, and in other countries worldwide.

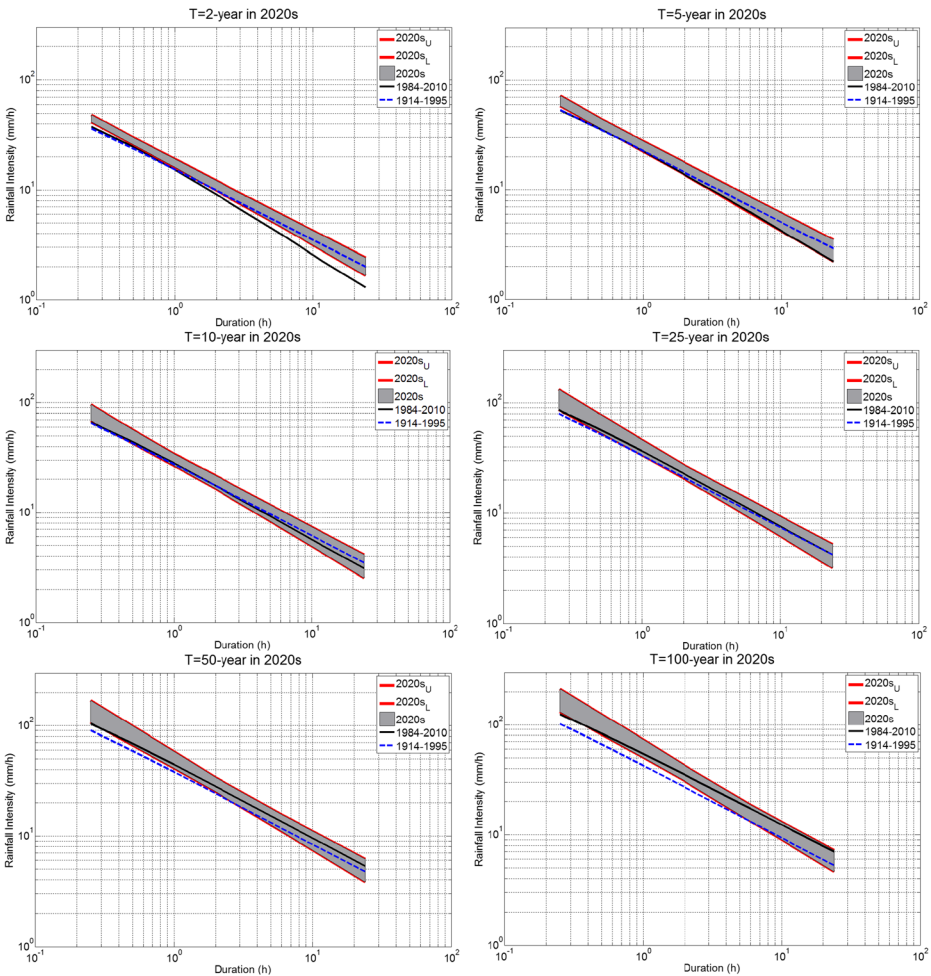


Fig. 3 Comparisons of past (1914–1995) IDF curves (blue dash line), current (1984–2010) IDF curves (black solid line), and MM5 projected (grey shaded area) IDF curves of the 2020s. Red lines stand for upper and lower bounds of projected IDF curves

Next, the present (1984–2010) IDF curves are compared with IDF curves projected for the 2020s (2011–2040), 2050s (2041–2070), and 2080s (2071–2100) (Figs. 3, 4 and 5), respectively. Apparently, more intensive storms are expected to occur in the future, especially for storms of short durations (≤ 1 -h). The projected IDF curves for 2020s (shaded grey) show higher intensities than that of the present (1984–2010) IDF curves (solid black curve) when the return periods are 2 and 5-years (Fig. 3). For return periods that are 10-year and above, only storms of short durations (≤ 1 -h) are projected to have consistently higher intensities. For longer storm durations (> 1 -h), the projected increase in intensities decreases as the return period increases (above 10-year). Overall, the highest increase in intensities projected are storms of 2-years return period, with a maximum increase of 89.6 %, a median increase of 22.4 %, and a minimum increase of 5 % over all durations and simulations. More details about the percentage change of projected rainfall intensities are listed in Table 1 and Tables S3–S5. The

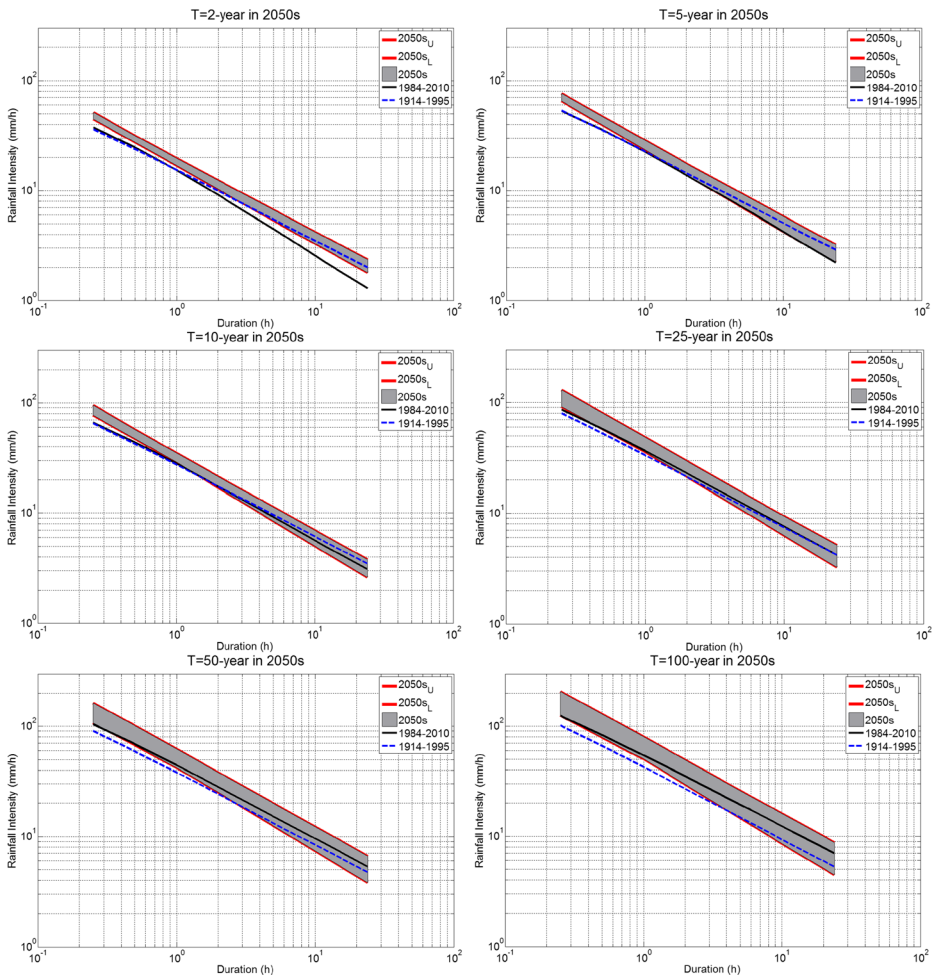


Fig. 4 Comparisons of past (1914–1995) IDF curves (blue dash line), current (1984–2010) IDF curves (black solid line), and MM5 projected (grey shaded area) IDF curves of the 2050s. Red lines stand for upper and lower bounds of projected IDF curves

maximum, median, and minimum percentage changes were derived from 10 sets of SRES projections.

Projected IDF curves for the 2050s and the 2080s (Figs. 4 and 5) generally exhibit higher projected intensities than those of the 2020s, e.g., higher median percentage change for the IDF curves of 2050s and 2080s than those of 2020s (Table 1). On a whole, storm intensities are projected to gradually increase from 2020s to 2080s for storms of short durations and return periods less than 25 years.

6 Summary and conclusions

Our results show that all three SRES scenarios, A2, A1B and B1 projected similar range of air temperature and precipitable water increase in central Alberta in the 2020s and the 2050s.

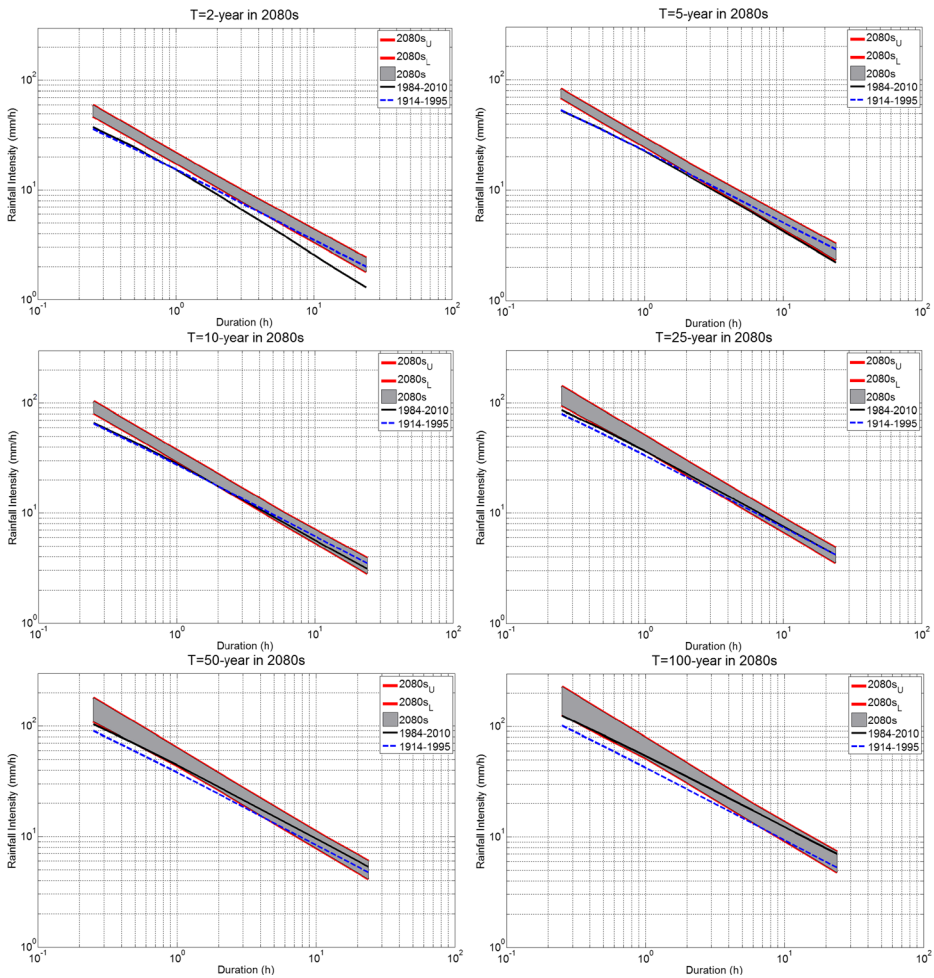


Fig. 5 Comparisons of past (1914–1995) IDF curves (blue dash line), current (1984–2010) IDF curves (black solid line), and MM5 projected (grey shaded area) IDF curves of the 2080s. Red lines stand for upper and lower bounds of projected IDF curves

However, for the 2080s, A2 and A1B scenarios project a higher increase in air temperature and precipitable water, but B1 scenario projects a relatively modest increase. The projected rate of air temperature increase ranges from 0.011 to 0.052 °C/year in 2011–2100. With reference to the climate normal of 1971–2000, air temperature of central Alberta is projected to increase by an average magnitude of about 2.9 °C in the 2080s. Consistent with the projected increase of air temperature, precipitable water is projected to increase at rates ranging from 0.125 to 0.485 %/year in 2011–2100, with an average increase of about 29 % by 2080s.

Based on projected IDF curves, it seems that future storms of central Alberta will gradually become more intensive, especially storms of short durations (≤ 1 -h). In some cases, the projected intensity for storms of short durations (≤ 1 -h) could increase up to 84.9 % in the 2080s. Further, for storms of low return periods (2 and 5-years), the projected intensities are consistently higher for all storm durations considered, and the projected increase ranges from 12.2 to 38.5 %.

Table 1 The maximum, median, and minimum changes (percentage) in the 2020s, 2050s, and 2080s with respect to 1984–2010, for return periods ranging from 2 to 100 years

Stage	Duration (h)	T=2 years			T=5 years			T=10 years			T=25 years			T=50 years			T=100 years		
		Min	Med	Max	Min	Med	Max	Min	Med	Max	Min	Med	Max	Min	Med	Max	Min	Med	Max
2020s	0.25	10.6	20.3	29.2	9.5	23.1	35.3	4.0	22.0	44.8	0.7	22.0	53.4	3.8	25.8	64.2	5.6	29.8	70.7
	0.5	5.0	13.7	22.0	1.6	13.7	24.3	-2.9	12.0	29.0	-5.7	13.0	36.4	-3.3	17.0	44.9	-2.6	19.9	49.3
	1	6.0	13.9	25.4	-1.0	9.3	23.0	-5.6	8.2	21.5	-8.8	9.8	25.4	-7.4	12.6	31.3	-8.0	13.6	33.6
	2	9.2	18.1	33.8	-0.4	8.9	26.8	-6.2	7.0	22.4	-10.1	8.5	19.1	-10.0	10.3	20.8	-12.1	9.1	21.1
	4	14.7	24.0	45.8	-1.3	9.2	32.9	-9.0	7.1	24.8	-12.9	8.3	20.0	-14.7	7.5	16.3	-19.2	4.1	10.5
	6	18.8	28.3	54.2	-1.6	9.7	37.3	-11.1	7.0	26.6	-15.7	7.7	20.9	-17.9	5.6	16.1	-23.0	2.1	7.9
2050s	12	24.5	36.7	70.7	-1.7	11.0	45.6	-14.4	5.7	30.2	-20.1	4.5	22.6	-23.1	-0.6	16.0	-28.9	-3.5	5.1
	24	30.1	46.9	89.6	-1.4	13.9	55.0	-17.3	4.6	34.1	-24.1	1.0	24.7	-27.9	-5.3	16.1	-34.3	-9.1	2.6
	0.25	19.7	28.7	36.9	23.1	30.9	42.7	16.8	31.3	43.7	6.5	31.7	50.2	3.6	33.0	58.7	0.7	34.7	67.2
	0.5	11.6	21.0	27.6	10.4	20.0	30.9	8.4	20.3	30.4	0.3	20.1	38.1	-2.0	21.3	47.1	-4.8	19.7	54.5
	1	10.5	19.8	28.8	4.0	15.5	26.4	3.0	14.1	24.3	-2.4	13.8	31.3	-4.7	14.3	40.0	-7.9	10.3	46.1
	2	13.5	22.5	35.9	1.0	14.0	25.9	-2.6	10.2	22.3	-6.8	8.6	27.1	-10.0	9.5	35.3	-15.6	4.9	40.0
2080s	4	19.2	28.0	46.6	-0.3	14.5	29.5	-6.7	7.9	21.8	-11.9	4.6	24.3	-15.9	4.7	31.7	-22.4	0.1	35.0
	6	23.3	32.0	54.0	-0.6	15.1	32.3	-8.7	6.8	21.9	-14.5	2.7	23.0	-19.0	1.7	29.9	-26.0	-3.7	32.4
	12	31.5	40.8	68.6	-0.6	16.8	37.8	-11.8	5.4	22.5	-18.6	-0.4	22.3	-23.9	-3.1	27.2	-31.7	-9.6	28.3
	24	40.7	51.8	85.3	-0.4	19.2	44.0	-14.6	4.7	23.3	-22.4	-1.6	22.7	-28.3	-5.7	24.7	-36.9	-12.5	24.4
	0.25	26.3	44.6	60.0	29.5	42.2	56.3	22.0	37.3	57.3	10.5	33.8	64.0	6.5	35.6	75.1	2.2	36.9	84.9
	0.5	16.9	31.7	46.7	15.9	28.7	40.4	12.0	26.0	42.1	3.9	22.4	47.8	1.2	23.9	56.4	-2.7	22.6	62.0
2080s	1	14.9	26.6	43.0	9.1	21.1	32.7	4.8	19.6	33.4	1.0	16.2	37.6	-1.2	15.7	43.5	-5.2	11.5	45.4
	2	17.3	27.2	46.5	5.9	18.1	29.9	0.3	15.9	28.2	-3.2	12.7	30.5	-6.1	9.7	33.7	-11.7	3.0	32.1
	4	22.3	30.9	55.5	4.5	17.3	32.7	-2.9	13.8	24.6	-7.3	8.9	25.1	-11.3	5.4	25.5	-18.3	-2.4	20.8
	6	26.1	33.9	62.0	4.2	17.4	35.0	-4.3	13.0	23.0	-9.3	7.0	22.3	-14.0	3.5	21.2	-21.7	-5.2	14.9
	12	33.5	41.1	74.6	4.1	18.0	39.7	-6.5	11.8	24.4	-12.6	4.1	18.0	-18.4	-0.7	15.4	-27.2	-8.5	8.8
	24	40.7	49.4	88.9	4.3	19.0	44.9	-8.5	10.2	26.3	-15.6	2.0	16.0	-22.4	-3.0	13.2	-32.2	-13.8	4.5

Return periods of short duration storms (≤ 1 -h) are projected to decrease greatly in 2011–2100, especially in 2041–2100. However, return periods of future storms of moderate durations, e.g., 4-h, could either increase or decrease while that of long duration storms, e.g., 24-h, tends to increase. Potentially, the projected increase of storm intensities imply that flooding in central Alberta due to the occurrence of severe storms of short durations could occur more frequently and in greater severity in future.

A quantile-quantile bias correction method was applied to correct the bias of simulated extreme storms of MM5. However, this bias correction approach is based on the assumption that the empirical relationship between the simulated and observed rainfall intensities will not change in future scenarios simulated by MM5. We selected climate projections of four GCMs of CMIP3 (Coupled Model Intercomparison Project Phase 3) for the projection of future IDF curves of central Alberta. Given that new climate change scenarios of the latest, higher resolution GCMs of IPCC known as Representative Concentration Pathways (RCPs) under the CMIP5 have only become available since 2013, any future extension of this study should be based on RCP scenarios of more GCMs to better assess uncertainties associated with long-term climate projections of GCMs. Ideally, instead of just using one RCM (MM5), future work should also include more RCMs to dynamically downscale climate scenarios of GCMs so that we can also assess uncertainties stemmed from RCMs selected for projecting climate change impact on future IDF curves.

Acknowledgments We are grateful to Compute Canada's WestGrid support staff for their assistance with technical issues of its supercomputers. This research was supported by the City of Edmonton and Natural Sciences and Engineering Research Council.

References

- Alexander LV et al (2006) Global observed changes in daily climate extremes of temperature and precipitation. *J Geophys Res* 111:D05109. doi:10.1029/2005JD006290
- Allan RP, Soden BJ (2008) Atmospheric warming and the amplification of precipitation extremes. *Science* 321: 1481–1484. doi:10.1126/science.1160787
- Boé J, Terray L, Habets F, Martin E (2007) Statistical and dynamical downscaling of the Seine basin climate for hydro-meteorological studies. *Int J Climatol* 27:1643–1655. doi:10.1002/joc.1602
- Christensen JH, Christensen OB (2003) Severe summertime flooding in Europe. *Nature* 421:805–806
- Dore MHI (2005) Climate change and changes in global precipitation patterns: what do we know? *Environ Int* 31:1167–1181. doi:10.1016/j.envint.2005.03.004
- Environment Canada (2014) The top ten Canadian weather stories for 2004–1. Storm drowns and pounds Edmonton. <https://www.ec.gc.ca/meteo-weather/default.asp?lang=En&n=9CA2BD37-1#top1>
- Erfani A, Methot A, Goodson R, Belair S, Yeh K, Cote J, Moffet R (2003) Synoptic and mesoscale study of a severe convective outbreak with the nonhydrostatic global environmental multiscale (GEM) model. *Meteorol Atmos Phys* 82:31–53. doi:10.1007/s00703-001-0585-8
- Groisman PY, Rankova EY (2001) Precipitation trends over the Russian permafrost-free zone: removing the artifacts of pre-processing. *Int J Climatol* 21:657–678. doi:10.1002/joc.627
- Hamlet AF, Lettenmaier DP (2007) Effects of 20th century warming and climate variability on flood risks in the western US. *Water Resour Res* 43:W06427. doi:10.1029/2006WR005099
- Hassanzadeh E, Nazemi A, Elshorbagy A (2014) Quantile-based downscaling of precipitation using genetic programming: application to IDF curves in Saskatoon. *J Hydrol Eng* 19(5):943–955. doi:10.1061/(ASCE)HE.1943-5584.0000854
- Hosking JRM, Wallis JR (1997) Regional frequency analysis: an approach based on L-moments. Cambridge University Press, New York
- Insurance Bureau of Canada (2012) Canadian severe weather – events and insured damage. http://www.abc.ca/en/Natural_Disasters/documents/2012_Insured_Damage/CDN_Insured_Damage.pdf
- IPCC Fifth Assessment Report: Working Group I (WGI) report (2013) Intergovernmental panel on climate change, Available from <http://www.ipcc.ch/>.

- IPCC Fourth Assessment Report: Working Group I (WGI) report (2007) Intergovernmental panel on climate change. Available from <http://www.ipcc.ch/>.
- Johnson F, Sharma A (2011) Accounting for interannual variability: a comparison of options for water resources climate change impact assessments. *Water Resour Res* 47:W04508. doi:10.1029/2010WR009272
- Kain JS (2004) The Kain–Fritsch convective parameterization: an update. *J Appl Meteorol Climatol* 43:170–181. doi:10.1175/1520-0450(2004)043<0170:TKCPAU>2.0.CO;2
- Kendall MG (1975) Rank correlation methods. Griffin, London
- Khon VC, Mokhov II, Roeckner E, Semenov VA (2007) Regional changes of precipitation characteristics in Northern Eurasia from simulations with global climate model. *Glob Planet Chang* 57(1–2):118–123. doi:10.1016/j.gloplacha.2006.11.006
- Kuo CC, Gan TY, Chan S (2013) Regional intensity-duration-frequency curves derived from ensemble empirical mode decomposition and scaling property. *J Hydrol Eng* 18:66–74. doi:10.1061/(ASCE)JHE.1943-5584.0000612
- Kuo CC, Gan TY, Hanrahan J (2014) Precipitation frequency analysis based on regional climate simulations in central Alberta. *J Hydrol* 510:436–446. doi:10.1016/j.jhydrol.2013.12.051
- Kyselý J, Beguería S, Beranová R, Gaál L, López-Moreno JI (2012) Different patterns of climate change scenarios for short-term and multi-day precipitation extremes in the Mediterranean. *Glob Planet Chang* 98–99:63–72. doi:10.1016/j.gloplacha.2012.06.010
- Lafon T, Dadson S, Buys G, Prudhomme C (2013) Bias correction of daily precipitation simulated by a regional climate model: a comparison of methods. *Int J Climatol* 33:1367–1381. doi:10.1002/joc.3518
- Laprise R, Caya D, Frigon A, Paquin D (2003) Current and perturbed climate as simulated by the second-generation Canadian regional climate model (CRCM-II) over northwestern north America. *Clim Dyn* 21:405–421. doi:10.1007/s00382-003-0342-4
- Lenderink G, Van Meijgaard E (2008) Increase in hourly precipitation extremes beyond expectations from temperature changes. *Nat Geosci* 1:511–514. doi:10.1038/ngeo262
- Mailhot A, Kingumbi A, Talbot G, Poulin A (2010) Future changes in intensity and seasonal pattern of occurrence of daily and multi-day annual maximum precipitation over Canada. *J Hydrol* 388:173–185. doi:10.1016/j.jhydrol.2010.04.038
- Mailhot A, Beaugard I, Talbot G, Caya D, Biner S (2012) Future changes in intense precipitation over Canada assessed from multi-model NARCCAP ensemble simulations. *Int J Climatol* 32:1151–1163. doi:10.1002/joc.2343
- Mann HB (1945) Nonparametric tests against trend. *Econometrica* 13:245–259
- Mekis E, Hogg WD (1999) Rehabilitation and analysis of Canadian daily precipitation time series. *Atmos Ocean* 37:53–85. doi:10.1080/07055900.1999.9649621
- Mladjic B, Sushama L, Khaliq MN, Laprise R, Caya D, Roy R (2011) Canadian RCM projected changes to extreme precipitation characteristics over Canada. *J Clim* 24:2565–2584. doi:10.1175/2010JCLI3937.1
- Mlawer EJ, Taubman SJ, Brown PD, Iacono MJ, Clough SA (1997) Radiative transfer for inhomogeneous atmospheres: RRTM, a validated correlated-k model for the longwave. *J Geophys Res* 102:16663–16682. doi:10.1029/97JD00237
- Reisner J, Rasmussen RM, Bruintjes RT (1998) Explicit forecasting of supercooled liquid water in winter storms using the MM5 mesoscale model. *Q J R Meteorol Soc* 124:1071–1107. doi:10.1002/qj.49712454804
- Sen PK (1968) Estimates of the regression coefficient based on Kendall's tau. *J Am Stat Assoc* 63:1379–1389
- Shepherd A, McGinn SM (2003) Assessment of climate change on the Canadian Prairies from downscaled GCM data. *Atmos Ocean* 41:301–316. doi:10.3137/ao.410404
- Shi X, Xu X (2008) Interdecadal trend turning of global terrestrial temperature and precipitation during 1951–2002. *Prog Nat Sci* 18:1383–1393. doi:10.1016/j.pnsc.2008.06.002
- Sillmann J, Kharin VV, Zwiers FW, Zhang X, Bronaugh D (2013) Climate extremes indices in the CMIP5 multimodel ensemble: part 2. Future climate projections. *J Geophys Res Atmos* 118:2473–2493. doi:10.1002/jgrd.50188
- Subash N, Singh SS, Priya N (2011) Extreme rainfall indices and its impact on rice productivity—a case study over sub-humid climatic environment. *Agric Water Manag* 98:1373–1387. doi:10.1016/j.agwat.2011.04.003
- Sun Y, Solomon S, Dai A, Portmann RW (2007) How often will it rain? *J Clim* 20:4801–4818. doi:10.1175/JCLI4263.1
- Sun F, Roderick ML, Lim WH, Farquhar GD (2011) Hydroclimatic projections for the Murray-darling basin based on an ensemble derived from intergovernmental panel on climate change AR4 climate models. *Water Resour Res* 47:W00G02. doi:10.1029/2010WR009829
- Theil H (1950) A rank-invariant method of linear and polynomial regression analysis. I, II, III. *Proceedings of the Koninklijke Nederlandse Akademie van Wetenschappen Series A* 53: 386–392, 521–525, 1397–1412
- Wang B, Bao Q, Hoskins B, Wu G, Liu Y (2008) Tibetan plateau warming and precipitation changes in east Asia. *J Geophys Res Lett* 35:L14702. doi:10.1029/2008GL034330

- Wang B, Zhang M, Wei J, Wang S, Li S, Ma Q, Li X, Pan S (2013) Changes in extreme events of temperature and precipitation over Xinjiang, northwest China, during 1960–2009. *Quat Int* 298:141–151. doi:[10.1016/j.quaint.2012.09.010](https://doi.org/10.1016/j.quaint.2012.09.010)
- Xu Y, Yang ZL (2012) A method to study the impact of climate change on variability of river flow: an example from the Guadalupe river in Texas. *Clim Chang* 113:965–979. doi:[10.1007/s10584-011-0366-4](https://doi.org/10.1007/s10584-011-0366-4)
- Zhang X, Vincent LA, Hogg WD, Niitsoo A (2000) Temperature and precipitation trends in Canada during the 20th century. *Atmos Ocean* 38:395–429. doi:[10.1080/07055900.2000.9649654](https://doi.org/10.1080/07055900.2000.9649654)